

## Growth mechanism study of silver nanostructures in a limited volume

D.V. Yakimchuk <sup>a</sup>, U.V. Prigodich <sup>a</sup>, S.E. Demyanov <sup>a</sup>, J. Ustarroz <sup>b,c</sup>, H. Terryn <sup>b</sup>, K. Baert <sup>b</sup>,  
S.A. Khubezhov <sup>d,e</sup>, D.I. Tishkevich <sup>a,f</sup>, A.V. Trukhanov <sup>a,f</sup>, V. Sivakov <sup>g</sup>, E.Yu. Kaniukov <sup>h</sup>

<sup>a</sup> Scientific-Practical Materials Research Centre of NAS of Belarus, 19 St. P.Brovka, 220072, Minsk, Belarus

<sup>b</sup> Vrije Universiteit Brussel, Pleinlaan 2, 1050 Brussels, Belgium

<sup>c</sup> Université libre de Bruxelles, Campus de la Plaine, Boulevard du Triomphe 2, CP 255. 1050, Brussels, Belgium

<sup>d</sup> Southern Federal University, 2 St. Shevchenko, 347922, Taganrog, Russian Federation

<sup>e</sup> ITMO University, 9 St. Lomonosova, 191002 St., Petersburg, Russian Federation

<sup>f</sup> South Ural State University, 76 St. Lenina, 454080, Chelyabinsk, Russian Federation

<sup>g</sup> Leibniz Institute of Photonic Technology, Albert-Einstein Str. 9, 07745, Jena, Germany

<sup>h</sup> National University of Science and Technology "MISIS", Leninskiy Prospekt 4, 119049, Moscow, Russian Federation

Recently, high attention has been paid to template synthesis as a method for obtaining nanostructures with predetermined shapes and sizes. This is an obvious approach, in which the size and shape of the pores limit the geometry of the nanostructures formed inside them. As a result, nanostructures completely repeat the shape of the template pores. In the presented work, we propose to consider another aspect of using a limited pore volume - as a tool for the formation of nanostructures with a predetermined morphology at diffusion-limited processes. Using silver as an example, it is shown that by changing only the pore volume, without changing other chemical kinetic conditions, it is possible to controllably create nanostructures with complex geometry. Possible morphologies of nanostructures, such as crystallites, dendrites and "sunflower-like" structures, formed at critical pore diameters, have been identified. The main points inherent to the formation of silver nanostructures in the pores of the SiO<sub>2</sub>/Si template using the electroless galvanic displacement method were highlighted. The growth mechanism of silver nanostructures in a limited pore volume has been studied and discussed in detail.

### Highlights

- The possibility of variation of the shape of Ag nanostructures only by changing the geometric parameters of the pore without changing other chemical kinetic conditions was demonstrated.
- By varying the pore volume of the template, Ag nanostructures like crystallites, dendrites and "sunflower-like" structures were formed. It was shown that, in the absence of pores, these types of nanostructures were not formed.
- The peculiarities of the evolution of crystallites, dendrites and "sunflower-like" structures were analyzed.

- The substantiation of the formation of Ag nanostructures of various types was suggested and the mechanism of their formation was proposed.

**Keywords:** Silver, Nanostructures, Porous template, Growth mechanism, Dendrites, Crystals

## Introduction

Due to their unique properties the nanostructures attract a special attention of researchers by applying various methods to create them. There are various approaches for their formation and the most common are a “top-down” and “bottom-up” ones [1,2]. It should be noted that the ‘top-down’ and ‘bottom-up’ methods for formation of nanomaterials are not mutually exclusive and often complement each other in the combined synthesis of nanostructures. One of the combined methods for creating nanostructures is a template synthesis, so-called due to the use of porous matrices (templates) in the preparation of nanomaterials with a given shape and size [3–5]. From the application point-of-view, both for research and for practical goals, the most commonly used templates are based on silicon [6], polymer films [7], as well as oxide materials such as  $\text{Al}_2\text{O}_3$  [8],  $\text{TiO}_2$  [9],  $\text{SiO}_2$  [10]. The overwhelming majority of works on the template synthesis of nanostructures are limited to the usage of a pore as a "mold" [11,12]. In this case, the pore volume does not allow the material to go beyond its boundaries, thereby determining the shape of the synthesized nanostructure, which completely repeats the pore shape [13–15].

It should be noted that an alternative approach for the controlled synthesis of nanostructures is also possible. In this approach, the shape of the synthesized nanostructures can be controlled by diffusion-limited process. The limited pore volume sets the direction of adatoms movement in the near-electrode layer provide to control the self-organization process aiming it in the desired direction. Thus, by changing the pore volume, in theory, it is possible to vary the shape of nanostructures in a wide range. Previously, we have already partially demonstrated the effectiveness of this approach in creating structures with complex morphologies of copper [16], silver [17], and gold nanostructures [18,19] in the pores of  $\text{SiO}_2/\text{Si}$  matrices. However, this approach to controlled synthesis of nanostructures has not yet received sufficient attention in the literature.

To eliminate this gap, in present work, we investigate the electroless galvanic displacement method during the self-assembly of silver nanostructures in a limited pore volume of  $\text{SiO}_2/\text{Si}$  template. Herein we show, the possibility to control the shape of the synthesized silver nanostructures only by changing the geometric (special) parameters of the pore without changing other chemical kinetic conditions. We determine the types of silver nanostructures morphologies can be formed during the self-organization of atoms nanostructures in a limited volume of a pore of  $\text{SiO}_2/\text{Si}$  template and describe the mechanism of their formation.

## Methods

There are three main approaches used to create templates: lithography [20], anodizing [9] and ion-track technology [21]. The advantages of templates created using ion-track technology include ease of adaptation to standard silicon technology processes and the ability to obtain templates with a large area. The main disadvantage is difficulties by obtaining ordered arrays of pores. Nevertheless, at the stage of creating and researching nanostructures, the use of ion-track templates becomes justified: it is possible to learn the main methodological approaches to obtaining nanostructures on a large scale.

As templates for synthesis of silver nanostructures, swift heavy ion-track porous SiO<sub>2</sub> template on *p*-type silicon substrate (12 Ohm·cm with orientation <100>) were used. The procedure of obtaining porous SiO<sub>2</sub>/Si templates are described in our previous paper [22]. The parameters of porous template as upper diameter  $D$ , lower diameter  $d$  and thickness of silicon oxide  $L$  were determined using ellipsometry [23,24]. Upper diameter  $D$  was in the range between 320 and 1000 nm, lower diameter  $d$  was in the range between 0 and 980 nm and thickness of silicon oxide  $L$  was in the range 25–500 nm. The SiO<sub>2</sub>/Si pore density over the surface was found to be  $5 \cdot 10^7 \text{ cm}^{-2}$  according SEM studies determined by ImageJ [25]. Characteristic SEM images and schematic representation of a pore in the SiO<sub>2</sub>/Si template is presented in Figure 1.

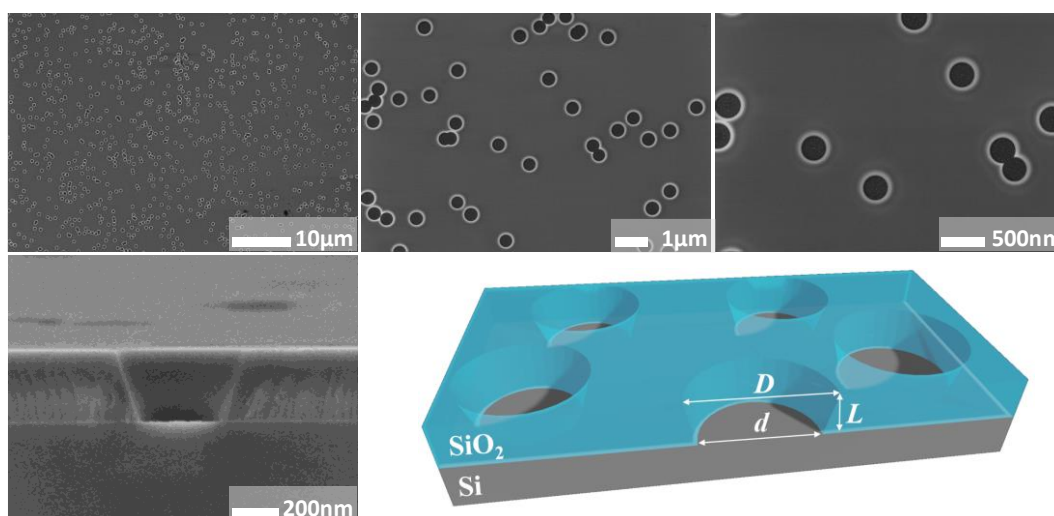


**Figure 1.** Typical SEM images of SiO<sub>2</sub>/Si template (planar and cross-section views) and schematic representation of a pore in the SiO<sub>2</sub>/Si template (upper diameter  $D$ , lower diameter  $d$  and thickness of silicon oxide  $L$ ).

The electroless galvanic displacement method [26] was used to localize silver in the pores of the amorphous silicon dioxide template. The deposition was carried out by immersing SiO<sub>2</sub>/Si templates in an aqueous solution containing 0.01 M silver nitrate (AgNO<sub>3</sub>) and 5 M hydrofluoric acid (HF). A temperature of 308K was set and controlled using a water bath, in which the electrolyte was thermostatted for 30 min. The deposition time was up to 60 s. The morphology of the SiO<sub>2</sub>(Ag)/Si surface was studied using JEOL JSM-7000F and Carl Zeiss ULTRA 55 field emission scanning electron microscopes (SEM).

## Results

SiO<sub>2</sub>/Si templates with different pore diameters were used as a pre-forming base for the synthesis of silver nanostructures. The pore diameter varied from the minimum ( $d = 0$ ,  $D_{\min} = 320$  nm) up to complete dissolution of the oxide layer. It should be noted that the deposition of metal into pores with different diameters with constant deposition parameters (temperature, deposition time, electrolyte composition) leads to the formation of nanostructures with dramatically different morphology as shown in Figure 2. The deposition of metal into pores with a minimal pore diameter  $D_{\min}$  (Figure 2a) leads to the formation of a precipitate only in some of them, leaving the rest of the pores either partially filled or unfilled at all. In templates with larger pore diameters, a fill rate of 100% is observed (Figure 2b-e).

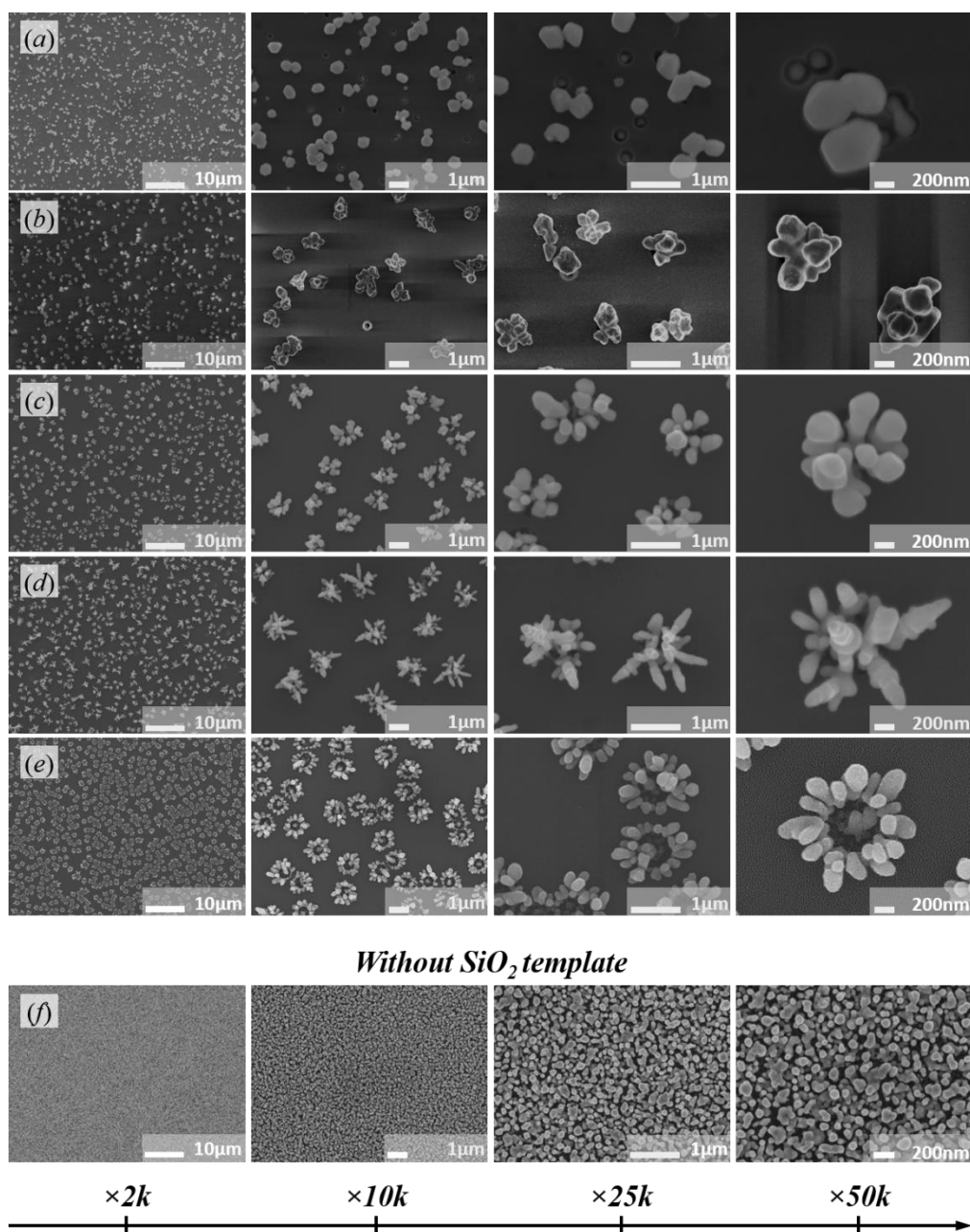


**Figure 2.** SEM images of silver nanostructures grown in SiO<sub>2</sub> pores with diameters  $D$  at the moment of pore opening (320 nm) (a); 400 nm (b); 600 nm (c); 750 nm (d); 950 nm (e) and after SiO<sub>2</sub> layer removing. for all samples was is 60 s

SEM studies provided in Fig.2 it is clearly seen that three main morphologies can be distinguished from the obtained structures: crystallites, dendrites and "sunflower-like" structures. An increase in the pore diameter leads to the change in the morphology of silver from crystallites at the moment of pore opening through intermediate forms of silver nanostructures to the most branched dendrites at  $D = 800$  nm and then to a "sunflower-like" structure at upper diameter of 1000 nm. It is important to note that when there is no porous  $\text{SiO}_2$  layer, the silicon surface is uniformly coated with silver nanoparticles without the formation of isolated nanostructures.

The obtained crystallites have characteristic sizes up to several micrometers. Pores  $D$  larger than 400 nm also contain structures with crystalline faces, but these faces are not as clearly distinguished as in the case of pores with  $D_{\text{min}}$ . With this  $D$ , nanostructures tend to grow with the formation of lateral processes ("dendritization"), while the sizes of the structures are in the range of 500-700 nm. At upper diameter values of 500 nm, the crystalline faces are not traced in the metal deposit, the structures have lateral dimensions of 600-900 nm and contain several branches. Nanostructures continue to grow with an increase in the pore diameter and at diameter of 800 nm the size of individual dendrites can reach 3  $\mu\text{m}$  as shown in Figure 2d. At diameter of 900 nm, despite a large number of separate branches, a cavity is formed in the central part of the structure, which, with a further increase in diameter to 1000 nm, modifies the metallic deposit to "sunflower-like" structures. In the central part of the "sunflower-like" structures, there is a deposit in the form of "tracks" of metal, similar to those obtained when silver is deposited on the free surface of silicon. Larger pores cannot be obtained with the specified etching parameters due to the complete dissolution of the  $\text{SiO}_2$  layer.

For detailed tracking of the evolving morphology of the silver deposit with a change in the pore diameter from the moment of pore opening to complete removal of the oxide layer, Figure 3 shows enlarged fragments of SEM images of individual silver nanostructures with a step of changing the upper diameter  $D$  of 100 nm.

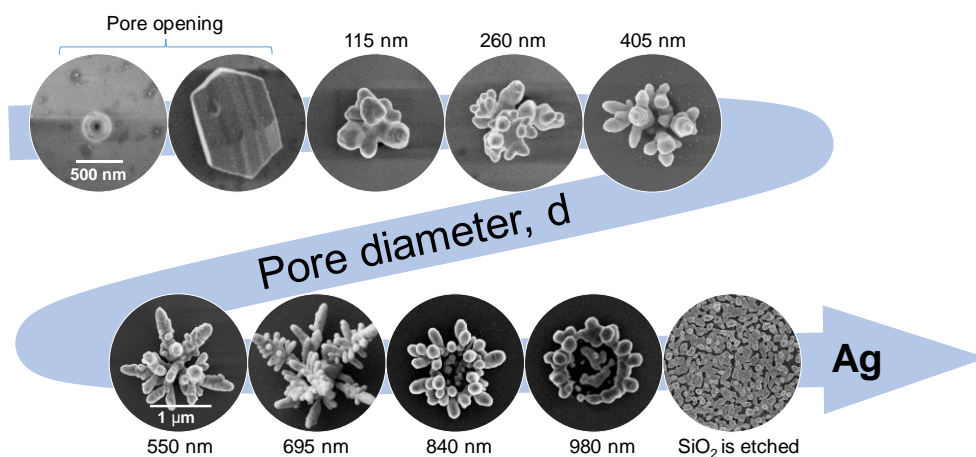


**Figure 3.** Dependence of the morphology of silver nanostructures on the pore diameter  $D$  of the  $\text{SiO}_2/\text{Si}$  template

The reasons for the formation of nanostructures with different morphologies with an increase in the pore diameter of the  $\text{SiO}_2/\text{Si}$  template can be understood by analyzing the evolving morphology

of the deposit during growth. For this, we studied the morphology of silver nanostructures at different stages of growth in template pores with different diameters. Typical SEM images are presented in Figure 4.

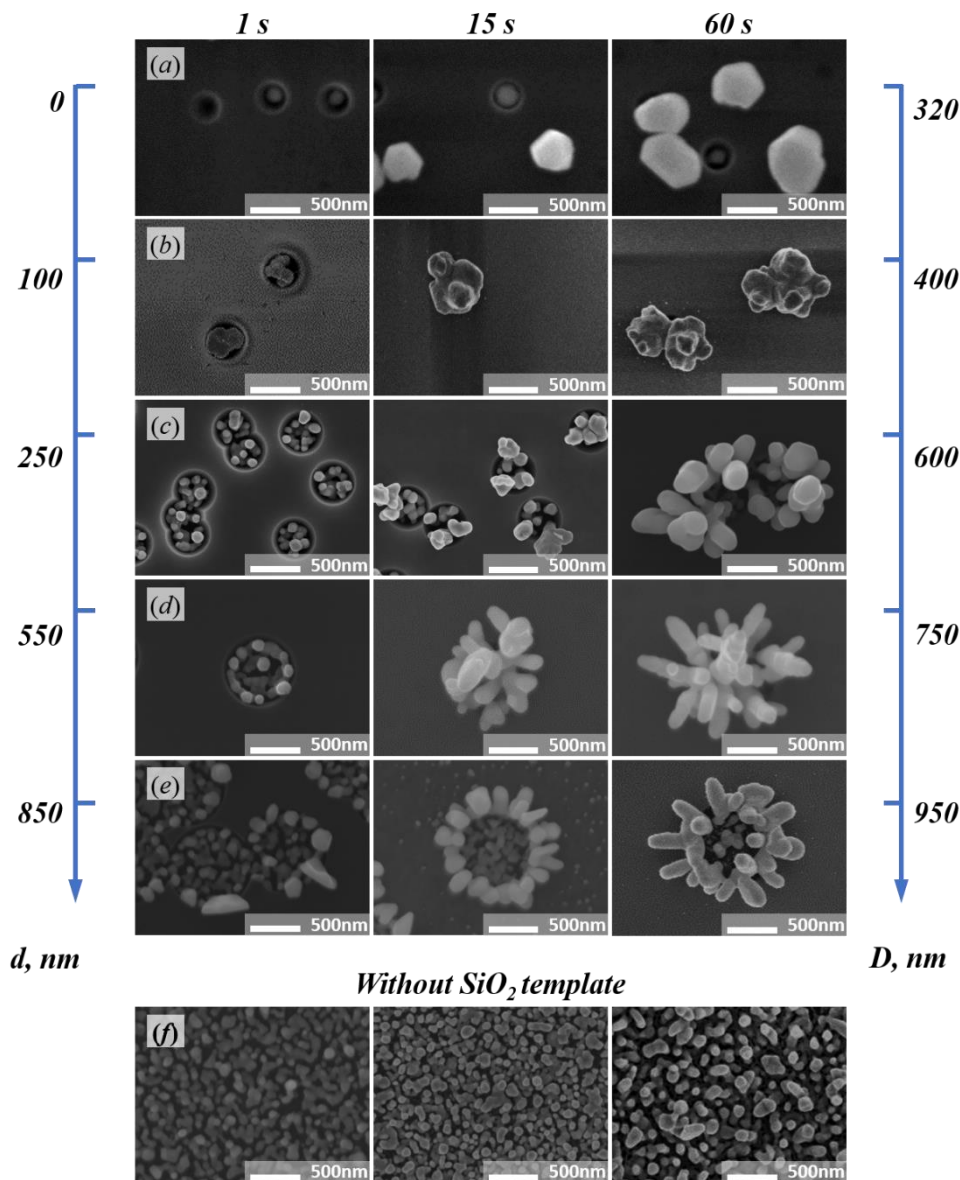


**Figure 4.** SEM planar images of silver nanostructures grown in  $\text{SiO}_2$  pores with diameters  $D$  at the moment of pore opening (320 nm (a); 400 nm (b); 600 nm (c); 750 nm (d); 950 nm (e) and after  $\text{SiO}_2$  layer removing. Deposition time is 1 s (left column), 15 s (middle column) and 60 s (right column)

It is clearly to see that at the final stage (deposition time 60 s) the obtained morphology strongly depends on the initial number of nuclei, which formed at the beginning of the process on the bottom of the pore (deposition time 1 s). The number of nuclei is determined by the pore diameters ( $D$  and  $d$ ). At  $d \approx 0$  and  $D = D_{\min}$  we have one nucleus at the start of the growing, which leads to the crystal obtaining (Figure 4a). At  $d = 100$  nm and  $D = 400$  nm the number of nuclei is about 3-4. The result is a growth of dense and randomly shaped silver crystallites (Figure 4b). An increased number of nuclei up to 10 ( $d = 250$  nm and  $D = 600$  nm) allows the formation of deposits in the form of several

“rod-like” silver crystals (Figure 4c). The limited pore volume together with the increased number of nuclei on average 18 ( $d = 550$  nm and  $D = 750$  nm), leads to the occurrence of diffusion-limited processes, as a result of which dendritization of the structures occurs (Figure 4d). At  $d = 850$  nm and  $D = 950$  nm the number of nuclei is increased due to the increase in the free area of the silicon surface. In this case, the growth is still limited by ion diffusion: the external parts of the structure are growing in a radial direction whereas the particles inside the pore do not grow because reactants do not reach them. As a result, we observe the formation of a “sunflower-like” structure (Figure 4e). The silver growth mechanism in SiO<sub>2</sub>/Si template will be described more in details below.

The growth of silver particles in the absence of SiO<sub>2</sub> pores on the free silicon surface is not accompanied by critical restrictions in local regions of the sample. Therefore, the evolution of the morphology of the deposit is of a usual character with a gradual increase in the volume of the particles (Figure 4f). Similar results for the deposition of silver onto a silicon surface using short deposition times (~ 3 minutes) or much longer deposition time (~15 minutes) and smaller AgNO<sub>3</sub> concentration (0.25 mM) have been previously reported in [27] and [28], respectively. It should be noted that an increasing the deposition time or AgNO<sub>3</sub> concentration in these works sometimes led to chaotic silver dendritization. In our work, we do not change these parameters.

## Discussion

*Electroless galvanic displacement of silver in pores of a SiO<sub>2</sub>/Si template.* To understand the mechanism of the growth of silver nanostructures in SiO<sub>2</sub>/Si template pores, it is necessary to understand which processes occur in the pore during the electroless galvanic displacement method. Information about the ongoing processes can be obtained by analyzing filled pores of the templates after the metal deposition process. Analysis of the filled templates in cross-sectional view after deposition of silver nanostructures in the pores of SiO<sub>2</sub> shows that during the formation of Ag precipitants by electroless galvanic displacement method the etching of silicon surface can take place as presented in Figure 5.

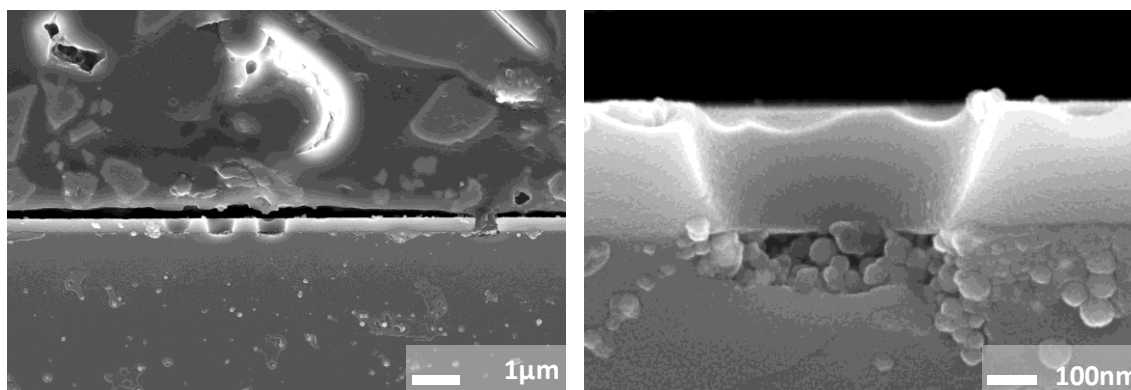
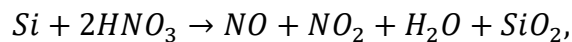
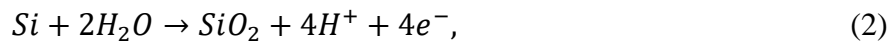


**Figure 5.** SEM cross-sectional view of the SiO<sub>2</sub>/Si template after deposition of silver nanostructures

Etching of a silicon surface during the electroless galvanic displacement method can occur for the following reasons. An aqueous solution of silver nitrate ( $\text{AgNO}_3$ ) and hydrofluoric acid (HF) dissociates in water into individual cations and anions ( $\text{Ag}^+$ ,  $\text{NO}_3^-$ ,  $\text{H}^+$ ,  $\text{F}^-$ ) [29]. The resulted ions participate in three parallel processes [30,31]: electrochemical reduction of  $[\text{Ag}]^+$  ions to a metallic silver state on Si or metal [Eq. (1)] with anodic oxidation of Si [Eq. (2)], and also  $\text{SiO}_2$  dissolution in hydrofluoric acid [Eq. (3)].



Schematically, the processes taking place in the pore of the  $\text{SiO}_2/\text{Si}$  template are presented in Figure 6.

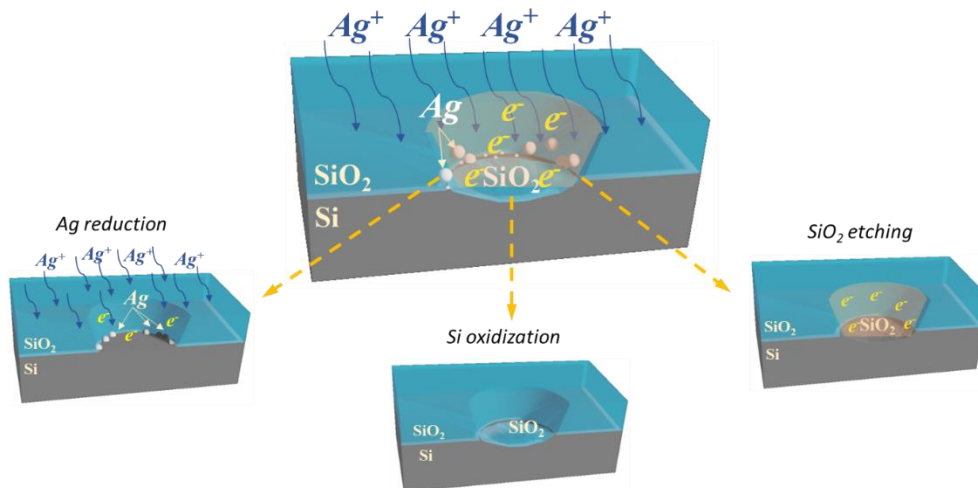


**Figure 6.** Schematic representation of the chemical processes involved in electrochemical reduction of silver ions occurring in pores of a  $\text{SiO}_2$  template on silicon

Thus, three chemical processes occur simultaneously in the pores. It should be noted that templates with different  $d$  and  $D$  implement different scenarios of these processes. Different scenarios occurring in local limited pore volumes lead to the growth of structures with different morphologies. Therefore, the growth mechanism should be considered depending on the pore diameters.

*Growth mechanism of silver structures in  $\text{SiO}_2/\text{Si}$  pores.* We will analyze, at what diameters ( $D$  and  $d$ ) the main morphologies are realized and describe the mechanism of growth of silver structures characteristic of each of these cases.  $D_{\min}$  ( $d < 50 \text{ nm}$ ). In this case, not all pores are open (etched to the silicon surface), i.e. when silver is deposited, the electrolyte will not react with the silicon substrate

in all pores. In an open pore, due to the interaction with the silicon substrate of the hydrofluoric acid included in the electrolyte, free electrons are formed. These electrons participate in the reduction of silver ions to the metallic state, as a result of which a metal nucleus is formed, which further determines the growth of the nanostructure. Considering the small size of the pore, a single growth center is formed at its bottom. Further development of the nanostructure is associated with the reduction of silver ions on this nucleus by the "metal on metal" mechanism [32]. Overtime (5-10 s), the pore is uniformly filled with metal, blocking the access of the electrolyte to silicon (cf. Figure 7 – Nucleation stage). However, the growth process continues: crystallites up to several micrometers in size appear above the surface of individual pores. The continuation of growth is due to the fact that the pores which were not initially opened are gradually etched into HF and “open”, providing an influx of electrons, some of which are distributed over the already existing Ag structures, increasing their size. Therefore, in Figure 7 (Middle and Final stages) individual silver crystallites of various sizes are observed on the surface of the SiO<sub>2</sub>/Si template.

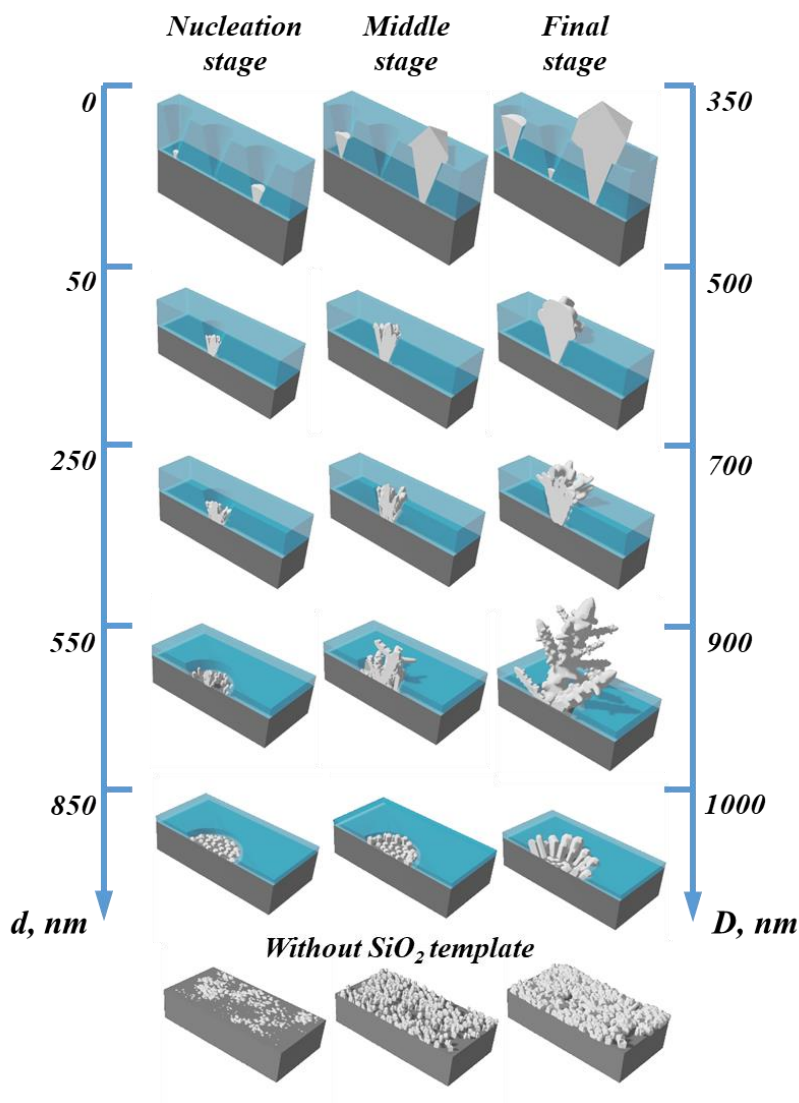


**Figure 7.** Schematic illustration of the stages of silver growth in pores SiO<sub>2</sub>/Si template at different pore diameters and without porous layer.

$350\text{ nm} < D < 500\text{ nm}$  ( $50\text{ nm} < d < 250\text{ nm}$ ). In this and subsequent cases, all the pores of the template are open, which ensures the formation of a silver precipitants in all pores. After "opening" the pore at the SiO<sub>2</sub>-Si interface, a contact area of the silicon substrate (naturally the silicon surface can provide four electrons, which can be used in the electrochemical processes) with the electrolyte is formed. The equilibrium nature of the electrodeless metal deposition process is realized due to the fact the electrons that reduce Ag<sup>+</sup> are coming permanently from the Si oxidation reaction [31,33,34] which happens at the bottom of the pore. Due to these localized processes occurring in a limited volume, a two-dimensional growth of the silver structure is realized inside the pore. The low growth rate of the silver deposit guarantees a sufficient rate of diffusion of silver ions to the nucleus inside the pore. After the metal leaves the upper boundary of the pore, the growth mechanism switches from two-dimensional to three-dimensional with the formation of a "cap" with characteristic crystal faces on the surface. The morphology (cf. Figure 7) of the structure is specified by the crystalline orientation of the metal deposit inside the pore.

$500\text{ nm} < D < 700\text{ nm}$  ( $250\text{ nm} < d < 550\text{ nm}$ ). An increase in the lower pore diameter leads to an increase in the number of electrons generated by the substrate, which determines the nonequilibrium nature of the metal reduction process due to the lack of silver ions in the cathode region. An insufficient amount of silver ions leads to the transformation of the crystal shape into a metal deposit of a complex shape (cf. Figure 7 – Nucleation stage). The deposit is evenly distributed over the surface due to the fact that the size of the contact area between silicon and electrolyte no longer plays such a significant role as at the moment of "opening" the pore. The number of nuclei formed at the bottom of the pore increases in proportion to the increase in the pore size. Their localization is carried out mainly along the edges of the pores and, in some cases, in the center (due to the defectiveness of the silicon surface in the center of the bottom of the pore, caused by the passage of swift heavy ions at the stage of creating a template during irradiation). In the process of growth, elongated metal structures (crystal rods) appear inside the pores, and after 5-10 s, the front of their growth overlaps. The contact and overlapping of the rods with each other lead to their accretion. In this case, a gap remains between them, which is sufficient for the penetration of the solution to the silicon substrate and the release of new electrons necessary for further growth of the structure (cf. Figure 7 – Middle stage). At the moment when the growth fronts overlap, there is competition for the electrolyte. After about 45 seconds, due to the rather dense filling of the pores and their complete coverage from above with a silver deposit, the influx of electrons stops, stopping the growth of the nanostructure (cf. Figure 7 – Final stage). The final form of the structures is influenced by the overlap of the growth fronts of individual crystals, and as a result, structures with crystal faces are formed, but less noticeable than in the previous case.

$700\text{ nm} < D < 900\text{ nm}$  ( $550\text{ nm} < d < 850\text{ nm}$ ). The growth process is similar to the previous

case, the difference is that with an increase in the lower diameter, it is possible to form a larger number of nuclei at the bottom of the pore. The presence of a larger number of competing growth centers within one pore leads to overlapping of their growth fronts during the development of the nanostructure, providing the formation of structures with complex geometry. Also, due to the increase in the free silicon surface at the bottom of the pore, more electrons are released, increasing the growth rate and providing the structure with large dimensions, and causing an increase in diffusion-limited processes with the implementation of the most branched morphology of silver (cf. Figure 7 – Middle stage). It should be noted that it is known several mechanisms for the growth of silver dendrites [35–38]. However, most researchers have agreed that the development of the dendritic structures is due to the anisotropic crystal growth and diffusion-limited aggregation [39,40]. Since the growth of dendrite occurs in a limited pore volume, where diffusion-limited processes are present, we will consider this mechanism in more detail. At the initial stage, the growth of silver particles is more efficient in the (111) direction, which leads to the formation of a dendrite trunk. Further growth occurs in an asymmetrical manner. This happens when the growth rate is limited by the rate of ion diffusion to the boundary of an already formed trunk. In the presence of a reducing agent,  $\text{Ag}^+$  ions are converted into nanoparticles that move randomly until they reach a low-energy position and attach to the trunk. The growth of attached particles also occurs in the (111) direction. Over time, the concentration gradient along the dendrite trunk changes, which leads to a change in the diffusion rate and, accordingly, to a more pronounced dendritization of the structure. In our case, the same diffusion-limited growth processes are realized in all pores of the sample, which leads to the formation of dendrites on the surface of the template (cf. Figure 7 – Final stage).

$900 \text{ nm} < D$  ( $850 \text{ nm} < d < 1000 \text{ nm}$ ). A further increase in the diameter leads to the fact that the growth of crystals nucleated at the edges of the pore is not accompanied by overlapping of their growth fronts. Nevertheless, growth competition arises due to the fact that the nuclei formed at the pore boundaries capture most of the incoming ions  $\text{Ag}^+$ . This leads to more intense growth of the structure at the edges of the pore and the formation of a thin silver deposit in its center, similar to a metal reduction on a free silicon surface. As a result, the pores of the template are filled with “sunflower-like” structures, consisting of individual crystallites that have grown on the sides of the pore (cf. Figure 7 – Final stage).

*Without porous  $\text{SiO}_2$  layer.* The deposition of silver under the same conditions on the free silicon surface does not provide a tool for regulating the rates of redox reactions, as well as the possibility of their controlled shift to the region of diffusion-limited processes, which explains the reason for the absence of a variety of morphologies of the metal deposit on a silicon substrate in the absence of a porous layer.

To summarize that was written above, it is worth highlighting the main points inherent in the

formation of silver nanostructures in the pores of the SiO<sub>2</sub>/Si template using the electroless galvanic displacement method:

*I.* The deposition of silver nanostructures in SiO<sub>2</sub> pores using the electroless galvanic displacement method involves three parallel processes:

1. Electrochemical reduction of Ag<sup>+</sup> ions to the state of metallic silver on Si or metal;
2. Anodic oxidation of Si;
3. Dissolution of SiO<sub>2</sub> in hydrofluoric acid.

*II.* Self-assembly of silver in a limited pore volume with forming of the hierarchical nanostructures is determined by the rate of diffusion-limited processes. The rate of the processes is set when choosing the pore diameter and determines the shape of the formed silver nanostructures.

*III.* By varying the pore diameter, the morphology of nanostructures can be changed over a wide range. However, from the nomenclature of the resulting structures, three main morphologies should be distinguished at the critical diameters:

1. Crystallites;
2. Dendrites;
3. "Sunflower-like" structures.

All other forms are intermediate variations of the indicated morphologies.

*IV.* In the absence of a porous SiO<sub>2</sub> layer, the silicon surface is uniformly coated with silver nanoparticles. No isolated nanostructures are formed.

Additionally, it should be noted that silver structures are promising for use in surface enhancement Raman spectroscopy to obtain a signal from low concentrations of the target molecule. For example, in our previous work [41] related to the implementation of similar nanostructures to the SERS platform, was shown that Ag nanostructures having the form of dendrites have the ability to detect an ultra-low concentration of the Ellman's reagent C<sub>14</sub>H<sub>8</sub>N<sub>2</sub>O<sub>8</sub>S<sub>2</sub> (5,50-dithiobis-(2-nitrobenzoic acid)), comparable to the concentrations of individual molecules. The high sensitivity of dendritic structures is associated with the presence of "hot spots" at the sites of twinning (coalescence of dendrite branches), where the electric field enhancement factor reaches 12. Also, similar silver dendrites structures were successfully implemented by electrochemical surface-enhanced Raman scattering [42–46].

However, structures that provide a high degree of amplification of the Raman signal can often have a damaging effect on the studied molecule due to too high-tension field in "hot spots", which leads to overheating and destruction of the molecule. The broad possibilities for controlling the morphology of nanostructures demonstrated in the present work will make it possible to obtain objects with the required shape and, accordingly, the required gain, which will make it possible to study substances without disturbing their molecular structure.

## Conclusions

The work was devoted to a detailed study of the influence of the geometric parameters of the template pores on the morphology of silver nanostructures. As a result of detailed studies of the diffusion-limited processes of self-assembly of a metal in a limited volume and relationship between the morphology of the metal deposit and the geometry of the pores of the SiO<sub>2</sub>/Si template it was shown that a change in the pore diameter makes it possible to predetermine the morphology of the metal deposit and create crystallites, dendrites, "sunflower-like" structures, as well as their intermediate configurations. A mechanism for the formation of nanostructures of silver with different morphologies in the pores of the SiO<sub>2</sub>/Si template is proposed.

## Acknowledgements

The reported study was funded by Belarusian Foundation for Basic Research [project number  $\Phi$ 21PM-054], Scientific-technical program 'Technology-SG' [project number 3.1.5.1], RFBR and BRFB project number 20-52-04015, and supported by the Ministry of Science and Higher Education of the Russian Federation; the state task in the field of scientific activity No. FENW-2022-0001. The authors also acknowledge the support of the work in frames of H2020 - MSCA - RISE2017 - 778308 - SPINMULTIFILM Project. V.S. gratefully acknowledges the financial support by the German Science Foundation (DFG) under contract number SI-1893/30-1.

## References

- [1] B.K. Teo, X.H. Sun, From Top-Down to Bottom-Up to Hybrid Nanotechnologies: Road to Nanodevices, *J. Clust. Sci.* 17 (2006) 529–540. <https://doi.org/10.1007/s10876-006-0086-5>.
- [2] P. Iqbal, J.A. Preece, P.M. Mendes, Nanotechnology: The "Top-Down" and "Bottom-Up" Approaches, in: *Supramol. Chem.*, John Wiley & Sons, Ltd, Chichester, UK, 2012: pp. 1–14. <https://doi.org/10.1002/9780470661345.smc195>.
- [3] D. Fink, A. V. Petrov, V. Rao, E. Al., Production parameters for the formation of metallic nanotubes in etched tracks, *Rad. Meas.* 36 (2003) 751.
- [4] L.D. De Pra, E. Ferain, R. Legras, E. Al., Fabrication of a new generation of track etched templates and their use for the synthesis of metallic and organic nanostructures, *Nucl. Instruments Methods Phys. Res. Sect. B Beam Interact. with Mater. Atoms.* 196 (2002) 81–88.
- [5] H. Yao, D. Mo, J. Duan, Y. Chen, J. Liu, Y. Sun, M. Hou, T. Schäpers, Investigation of the surface properties of gold nanowire arrays, *Appl. Surf. Sci.* 258 (2011) 147–150. <https://doi.org/10.1016/j.apsusc.2011.08.021>.
- [6] L. Boarino, S. Borini, G. Amato, Electrical Properties of Mesoporous Silicon: From a Surface Effect to Coulomb Blockade and More, *J. Electrochem. Soc.* 156 (2009) K223–K226. <https://doi.org/10.1149/1.3232202>.
- [7] P. Guo, C.R. Martin, Y. Zhao, J. Ge, R.N. Zare, General method for producing organic nanoparticles using nanoporous membranes, *Nano Lett.* 10 (2010) 2202–2206. <https://doi.org/10.1021/nl101057d>.
- [8] N.A. Kalanda, G.G. Gorokh, M. V. Yarmolich, A.A. Lozovenko, E.Y. Kanyukov, Magnetic and magnetoresistive

- properties of Al<sub>2</sub>O<sub>3</sub>-Sr<sub>2</sub>FeMoO<sub>6</sub>- $\delta$ -Al<sub>2</sub>O<sub>3</sub> nanoheterostructures, *Phys. Solid State.* 58 (2016) 351–359. <https://doi.org/10.1134/S1063783416020128>.
- [9] A. Cultrera, L. Boarino, G. Amato, C. Lamberti, Band-gap states in unfilled mesoporous nc-TiO<sub>2</sub>: measurement protocol for electrical characterization, *J. Phys. D. Appl. Phys.* 47 (2014) 015102 (1–8). <https://doi.org/10.1088/0022-3727/47/1/015102>.
- [10] A. Dallanora, T.L. Marcondes, G.G. Bermudez, P.F.P. Fichtner, C. Trautmann, M. Toulemonde, R.M. Papaléo, Nanoporous SiO<sub>2</sub>/Si thin layers produced by ion track etching: Dependence on the ion energy and criterion for etchability, *J. Appl. Phys.* 104 (2008) 024307-1-024307–8. <https://doi.org/10.1063/1.2957052>.
- [11] M. Celik, F. Buyukserin, The use of anodized alumina molds for the fabrication of polymer nanopillar arrays as SERS substrates with tunable properties, *Vib. Spectrosc.* 104 (2019) 102965. <https://doi.org/10.1016/j.vibspec.2019.102965>.
- [12] S.Y. Kang, C.W. Kang, D.W. Kim, Y. Myung, J. Choi, S.M. Lee, H.J. Kim, Y. Ko, S.U. Son, Colloidal Template Synthesis of Nanomaterials by Using Microporous Organic Nanoparticles: The Case of C@MoS<sub>2</sub> Nanoadsorbents, *Chem. – An Asian J.* 14 (2019) 3173–3180. <https://doi.org/10.1002/asia.201900885>.
- [13] Z. Li, F. Gao, Z. Gu, Vertically aligned Pt nanowire array/Au nanoparticle hybrid structure as highly sensitive amperometric biosensors, *Sensors Actuators B Chem.* 243 (2017) 1092–1101. <https://doi.org/10.1016/j.snb.2016.12.033>.
- [14] J. Wang, Z. Li, F. Gao, H. Sun, Z. Gu, Infrared (IR) irradiation induced surface and morphology changes in Sn-based multi-segmented metallic nanowires, *Nano-Structures & Nano-Objects.* 23 (2020) 100492. <https://doi.org/10.1016/j.nanoso.2020.100492>.
- [15] J. Wang, Z. Li, Z. Gu, A comprehensive review of template-synthesized multi-component nanowires: From interfacial design to sensing and actuation applications, *Sensors and Actuators Reports.* 3 (2021) 100029. <https://doi.org/10.1016/j.snr.2021.100029>.
- [16] E. Kaniukov, D. Yakimchuk, G. Arzumanyan, H. Terryn, K. Baert, A. Kozlovskiy, M. Zdorovets, E. Belonogov, S. Demyanov, Growth mechanisms of spatially separated copper dendrites in pores of a SiO<sub>2</sub> template, *Philos. Mag.* 97 (2017). <https://doi.org/10.1080/14786435.2017.1330562>.
- [17] D.V. Yakimchuk, E.Y. Kaniukov, S. Lepeshov, V.D. Bundyukova, S.E. Demyanov, G.M. Arzumanyan, N.V. Doroshkevich, K.Z. Mamatkulov, A. Bochmann, M. Presselt, O. Stranik, S.A. Khubezhov, A.E. Krasnok, A. Alù, V.A. Sivakov, Self-organized spatially separated silver 3D dendrites as efficient plasmonic nanostructures for surface-enhanced Raman spectroscopy applications, *J. Appl. Phys.* 126 (2019). <https://doi.org/10.1063/1.5129207>.
- [18] D. V. Yakimchuk, V.D. Bundyukova, J. Ustarroz, H. Terryn, K. Baert, A.L. Kozlovskiy, M. V. Zdorovets, S.A. Khubezhov, A. V. Trukhanov, S. V. Trukhanov, L. V. Panina, G.M. Arzumanyan, K.Z. Mamatkulov, D.I. Tishkevich, E.Y. Kaniukov, V. Sivakov, Morphology and Microstructure Evolution of Gold Nanostructures in the Limited Volume Porous Matrices, *Sensors.* 20 (2020) 4397. <https://doi.org/10.3390/s20164397>.
- [19] L.A. Osminkina, O. Žukovskaja, S.N. Agafilushkina, E. Kaniukov, O. Stranik, K.A. Gonchar, D. Yakimchuk, V. Bundyukova, D.A. Chermoshentsev, S.A. Dyakov, N.A. Gippius, K. Weber, J. Popp, D. Cialla-May, V. Sivakov, Gold nanoflowers grown in a porous Si/SiO<sub>2</sub> matrix: The fabrication process and plasmonic properties, *Appl. Surf. Sci.* 507 (2020) 144989. <https://doi.org/10.1016/j.apsusc.2019.144989>.
- [20] M.J. Kim, M. Wanunu, D.C. Bell, A. Meller, Rapid fabrication of uniformly sized nanopores and nanopore arrays for parallel DNA analysis, *Adv. Mater.* 18 (2006) 3149–3153. <https://doi.org/10.1002/adma.200601191>.
- [21] D. Fink, A. V. Petrov, K. Hoppe, W.R. Fahrner, R.M. Papaleo, A.S. Berdinsky, A. Chandra, A. Chemseddine, A. Zrineh, A. Biswas, F. Faupel, L.T. Chadderton, Etched ion tracks in silicon oxide and silicon oxynitride as charge injection or extraction channels for novel electronic structures, *Nucl. Instruments Methods Phys. Res. B.* 218 (2004) 355–361.

<https://doi.org/10.1016/j.nimb.2003.12.083>.

- [22] E.Y. Kaniukov, J. Ustarroz, D. V Yakimchuk, M. Petrova, H. Terryn, V. Sivakov, A. V Petrov, Tunable nanoporous silicon oxide templates by swift heavy ion tracks technology, *Nanotechnology*. 27 (2016) 115305. <https://doi.org/10.1088/0957-4484/27/11/115305>.
- [23] V. Bundyukova, E. Kaniukov, A. Shumskaya, A. Smirnov, M. Kravchenko, D. Yakimchuk, Ellipsometry as an express method for determining the pore parameters of ion-track SiO<sub>2</sub> templates on a silicon substrate, *EPJ Web Conf.* 201 (2019) 01001. <https://doi.org/10.1051/epjconf/201920101001>.
- [24] D. Yakimchuk, V. Bundyukova, A. Smirnov, E. Kaniukov, Express Method of Estimation of Etched Ion Track Parameters in Silicon Dioxide Template, *Phys. Status Solidi*. 256 (2019) 1800316. <https://doi.org/10.1002/pssb.201800316>.
- [25] V. Bundyukova, D. Yakimchuk, E. Shumskaya, A. Smirnov, M. Yarmolich, E. Kaniukov, Post-processing of SiO<sub>2</sub>/Si ion-track template images for pores parameters analysis, *Mater. Today Proc.* 7 (2019) 828–834. <https://doi.org/10.1016/j.matpr.2018.12.081>.
- [26] C.N. Grabill, D. Freppon, M. Hettinger, S.M. Kuebler, Nanoscale morphology of electrolessly deposited silver metal, *Appl. Surf. Sci.* 466 (2019) 230–243. <https://doi.org/10.1016/j.apsusc.2018.10.006>.
- [27] P.R. Brejna, P.R. Griffiths, Electroless Deposition of Silver Onto Silicon as a Method of Preparation of Reproducible Surface-Enhanced Raman Spectroscopy Substrates and Tip-Enhanced Raman Spectroscopy Tips, *Appl. Spectrosc.* 64 (2010) 493–499. <https://doi.org/10.1366/000370210791211682>.
- [28] T.C. Dao, T.Q.N. Luong, T.A. Cao, N.M. Kieu, V.V. Le, Application of silver nanodendrites deposited on silicon in SERS technique for the trace analysis of paraquat, *Adv. Nat. Sci. Nanosci. Nanotechnol.* 7 (2016) 015007. <https://doi.org/10.1088/2043-6262/7/1/015007>.
- [29] D. Yakimchuk, E. Kaniukov, V. Bundyukova, L. Osminkina, S. Teichert, S. Demyanov, V. Sivakov, Silver nanostructures evolution in porous SiO<sub>2</sub>/p-Si matrices for wide wavelength surface-enhanced Raman scattering applications, *MRS Commun.* 8 (2018) 95–99. <https://doi.org/10.1557/mrc.2018.22>.
- [30] M. Abouda-Lachiheb, N. Nafie, M. Bouaicha, The dual role of silver during silicon etching in HF solution, *Nanoscale Res. Lett.* 7 (2012) 455. <https://doi.org/10.1186/1556-276X-7-455>.
- [31] W. Ye, Y. Chang, C. Ma, B. Jia, G. Cao, C. Wang, Electrochemical investigation of the surface energy: Effect of the HF concentration on electroless silver deposition onto p-Si (111), *Appl. Surf. Sci.* 253 (2007) 3419–3424. <https://doi.org/10.1016/j.apsusc.2006.07.049>.
- [32] S. Xie, X. Zhang, S. Yang, M.C. Paa, D. Xiao, M.M.F. Choi, Liesegang rings of dendritic silver crystals emerging from galvanic displacement reaction in a liquid-phase solution, *RSC Adv.* 2 (2012) 4627–4631. <https://doi.org/10.1039/C2RA20055D>.
- [33] T. Qiu, X.L. Wu, G.G. Siu, P.K. Chu, Intergrowth mechanism of silicon nanowires and silver dendrites, *J. Electron. Mater.* 35 (2006) 1879–1884. <https://doi.org/10.1007/s11664-006-0171-4>.
- [34] K. Drozdowicz-Tomsia, F. Xie, E.M. Goldys, Deposition of silver dendritic nanostructures on silicon for enhanced fluorescence, *J. Phys. Chem. C*. 114 (2010) 1562–1569. <https://doi.org/10.1021/jp9114942>.
- [35] M. V. Mandke, S.-H. Han, H.M. Pathan, Growth of silver dendritic nanostructures via electrochemical route, *CrystEngComm*. 14 (2012) 86–89. <https://doi.org/10.1039/C1CE05791J>.
- [36] E. Ben-Jacob, P. Garik, The formation of patterns in non-equilibrium growth, *Nature*. 343 (1990) 523–530. <https://doi.org/10.1038/343523a0>.
- [37] T. Haxhimali, A. Karma, F. Gonzales, M. Rappaz, Orientation selection in dendritic evolution, *Nat. Mater.* 5 (2006) 660–664. <https://doi.org/10.1038/nmat1693>.

- [38] C. Zhang, Y. Lu, B. Zhao, Y. Hao, Y. Liu, Facile fabrication of Ag dendrite-integrated anodic aluminum oxide membrane as effective three-dimensional SERS substrate, *Appl. Surf. Sci.* 377 (2016) 167–173. <https://doi.org/10.1016/j.apsusc.2016.03.132>.
- [39] T.A. Witten, L.M. Sander, Diffusion-Limited Aggregation, a Kinetic Critical Phenomenon, *Phys. Rev. Lett.* 47 (1981) 1400–1403. <https://doi.org/10.1103/PhysRevLett.47.1400>.
- [40] M.M. Alam, W. Ji, H.N. Luitel, Y. Ozaki, T. Watari, K. Nakashima, Template free synthesis of dendritic silver nanostructures and their application in surface-enhanced Raman scattering, *RSC Adv.* 4 (2014) 52686–52689. <https://doi.org/10.1039/C4RA10113H>.
- [41] D. V. Yakimchuk, E.Y. Kaniukov, S. Lepeshov, V.D. Bundukova, S.E. Demyanov, G.M. Arzumanyan, N. V. Doroshkevich, K.Z. Mamatkulov, A. Bochmann, M. Presselt, O. Stranik, S.A. Khubezhov, A.E. Krasnok, A. Alù, V.A. Sivakov, Self-organized spatially separated silver 3D dendrites as efficient plasmonic nanostructures for surface-enhanced Raman spectroscopy applications, *J. Appl. Phys.* 126 (2019) 233105. <https://doi.org/10.1063/1.5129207>.
- [42] Z. Wang, Z. Zhao, J. Qiu, A general strategy for synthesis of silver dendrites by galvanic displacement under hydrothermal conditions, *J. Phys. Chem. Solids.* 69 (2008) 1296–1300. <https://doi.org/10.1016/j.jpcs.2007.10.089>.
- [43] B. Zhao, Y. Lu, C. Zhang, Y. Fu, S. Moeendarbari, S.R. Shelke, Y. Liu, Y. Hao, Silver dendrites decorated filter membrane as highly sensitive and reproducible three dimensional surface enhanced Raman scattering substrates, *Appl. Surf. Sci.* 387 (2016) 431–436. <https://doi.org/10.1016/j.apsusc.2016.06.128>.
- [44] F.H. Cho, Y.C. Lin, Y.H. Lai, Electrochemically fabricated gold dendrites with high-index facets for use as surface-enhanced Raman-scattering-active substrates, *Appl. Surf. Sci.* 402 (2017) 147–153. <https://doi.org/10.1016/j.apsusc.2017.01.055>.
- [45] J. Raveendran, A. Docoslis, Portable surface-enhanced Raman scattering analysis performed with microelectrode-templated silver nanodendrites, *Analyst.* 145 (2020) 4467–4476. <https://doi.org/10.1039/D0AN00484G>.
- [46] D. Ibáñez, M.B. González-García, D. Hernández-Santos, P. Fanjul-Bolado, Detection of dithiocarbamate, chloronicotiny and organophosphate pesticides by electrochemical activation of SERS features of screen-printed electrodes, *Spectrochim. Acta Part A Mol. Biomol. Spectrosc.* 248 (2021) 119174. <https://doi.org/10.1016/j.saa.2020.119174>.